

Absolute frequency measurement of $^1S_0 (F = 1/2) - ^3P_0 (F = 1/2)$ transition of ^{171}Yb atoms in a one-dimensional optical lattice at KRISS

Chang Yong Park, Dai-Hyuk Yu*, Won-Kyu Lee, Sang Eon Park, Eok Bong Kim, Sun Kyung Lee, Jun Woo Cho, Tai Hyun Yoon**, Jongchul Mun, Sung Jong Park, Taeg Yong Kwon, and Sang-Bum Lee

Korea Research Institute of Standards and Science, Daejeon 305-340, Korea

*Corresponding author e-mail: dhyu@kriss.re.kr

**Current address: Department of Physics, Korea University, Seoul 136-713, Korea

Abstract

We measured the absolute frequency of the optical clock transition $^1S_0 (F = 1/2) - ^3P_0 (F = 1/2)$ of ^{171}Yb atoms confined in a one-dimensional optical lattice and it was determined to be 518 295 836 590 865.7 (9.2) Hz. The measured frequency was calibrated to the Coordinated Universal Time (UTC) by using an optical frequency comb of which frequency was phase-locked to a hydrogen maser as a flywheel oscillator traceable to the UTC. The magic wavelength was also measured as 394 798.48 (79) GHz. The results are in good agreement with two previous measurements of other institutes within the specified uncertainty of this work.

1. Introduction

Recently optical clocks based on narrow optical transitions of neutral atoms in an optical lattice [1-23] or a single ion in a Paul trap [24-26] have proved their potential capability to reach uncertainty level below 10^{-17} , and some of them already surpassed the best microwave clocks in the stability and systematic uncertainty [27-29]. Compared to optical ion clocks, optical lattice clocks are expected to have much better short-term stability with a large number of atoms interrogated, which may lead to much smaller quantum projection noise. Sr [1-11], Yb [12-19], Hg [20-22], Mg [23] atoms are actively investigated for future optical lattice clocks in many institutes worldwide.

Among these elements, Yb has several merits as an optical lattice clock. Natural abundance of Yb isotopes is reasonably distributed over bosonic and fermionic isotopes. Adequate transitions exist for manipulating atoms in ultracold state. Furthermore, solid state lasers are available for all related processes to investigate the clock transition [30-32]. Ytterbium optical lattice clocks using a bosonic isotope (^{174}Yb) were first realized with the magnetically-induced spectroscopy method [12-15]. Fermionic ^{171}Yb atoms were also actively studied with a merit of reduced collision shift due to the Pauli exclusion principle. Additionally, the simplest spin-1/2 system provides effective single-stepped optical pumping between Zeeman sub-levels for preparing spin-polarized ensemble of atoms and the frequency shift associated with the tensor polarizability induced by the lattice electric field is intrinsically removed.

Currently at least five groups are studying ^{171}Yb optical lattice clock to our knowledge and two groups reported measurement results on the absolute frequency of the clock transition [17, 18]. Frequency comparison between laboratories plays a crucial role in the discussion of the next generation frequency standard, since independent measurements in many laboratories are required to confirm that there are no remaining systematic errors as in the case of Sr optical lattice clock [1-11]. In this paper we report the third independent absolute frequency measurement result, to our knowledge, of the optical clock transition of ^{171}Yb atoms in a one dimensional (1-D) optical lattice. Frequency shifts due to the optical

lattice, Zeeman effect, blackbody radiation, collisions between trapped atoms, and gravitational effect were investigated to evaluate the shifts and systematic uncertainties. The absolute frequency was measured using an optical frequency comb, which was referenced to a H-maser as a flywheel oscillator. With the final correction of the H-maser frequency-offset against the Coordinated Universal Time (UTC), the absolute frequency of the transition was determined to be 518 295 836 590 865.7 Hz, with an uncertainty of 9.2 Hz (1.8×10^{-14}). This result agrees well with the two previous measurements performed by other laboratories within the uncertainty of this work.

In section 2, the whole experimental scheme and laser systems are overviewed. In section 3, the systematic shifts and the uncertainties of this measurement are discussed. In section 4, the absolute frequency is determined with the total uncertainty including the systematic uncertainty, the statistical uncertainty, and the uncertainty related to the link to the UTC. In section 5, conclusions and future plans are given.

2. Experiment

The clock transition $^1S_0(F=1/2) - ^3P_0(F=1/2)$ and other relevant energy levels of ^{171}Yb atoms are depicted in Fig. 1. The strong transition of $^1S_0(F=1/2) - ^1P_1(F=3/2)$ at 399 nm was used for Zeeman slower and first stage magneto-optical trap (blue-MOT). Then the transition of $^1S_0(F=1/2) - ^3P_1(F=3/2)$ at 556 nm was used for the deep cooling (green-MOT) to prepare Yb atoms in a 1-D optical lattice providing the Lamb-Dicke condition. The lattice laser at 759 nm was tuned to the magic wavelength determined experimentally, at which the Stark shift due to the optical lattice becomes zero. The clock transition was interrogated with a clock laser with the help of the electron shelving [33] and repumping techniques to accurately measure the population of the excited state and the ground state. Two repumping lasers at 649 nm and 770 nm were used for this purpose. Using this information, the spectrum of the clock transition was normalized with a good signal-to-noise ratio (SNR).

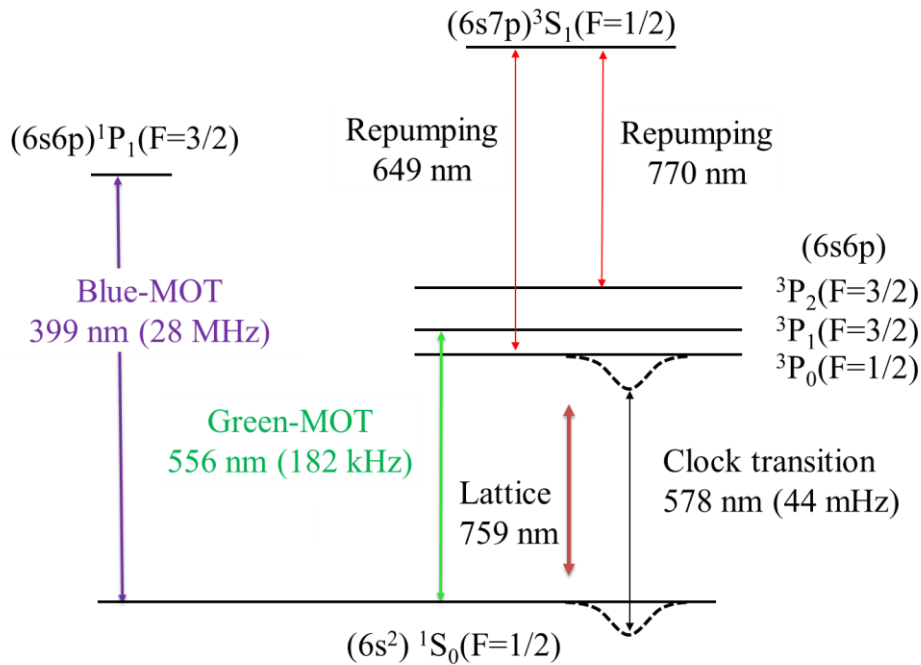


Figure 1. Relevant energy levels of ^{171}Yb atoms and lasers to drive various transitions. Lasers for optical lattice (759 nm), clock transition (578 nm), two cooling transitions (399 nm and 556 nm), and two repumping transitions (650 nm and 770 nm). Natural linewidths of the cooling transitions and the clock transition are given in parentheses.

2.1 Laser systems

In Fig. 2, the schematic diagram of the experimental setup is depicted. The laser system for the Zeeman slower and the blue-MOT consists of two Fabry-Pérot diode lasers (F-P LD's in Fig. 2) (NICHIA; NDV4313; 120 mW, 400~401 nm wavelength selected) injection-locked by a master external-cavity diode laser (ECDL). The slave lasers kept at 13°C were seeded with injection power of 1 mW. The frequency of the master ECDL was locked to the fluorescence signal of the $^1S_0(F=1/2) - ^1P_1(F=3/2)$ transition obtained from an atomic beam. The frequency detuning of the blue-MOT beam was adjusted by varying the intersection angle between the master laser and the collimated atomic beam for the best trap efficiency. The frequency of the seed laser for the Zeeman slower was shifted by -500 MHz from the resonance of the transition through a double-pass acousto-optic modulator (AOM). Both slave lasers had the output power of 40 mW, which were at the level of 70~80% of the full power to increase the lifetimes of laser diodes.

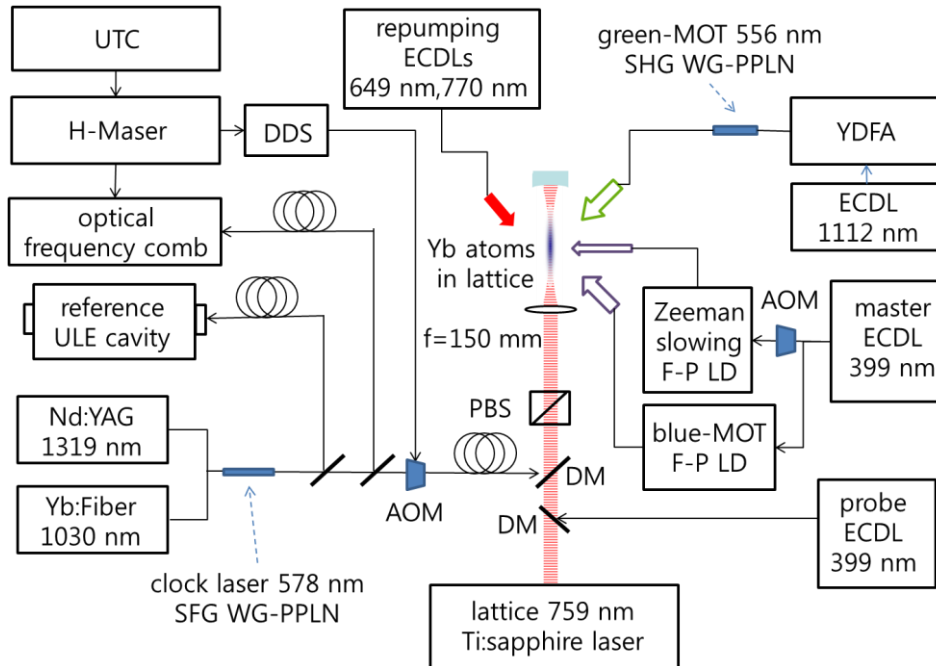


Figure 2. Schematic diagram of the experimental setup. 759-nm (lattice), 578-nm (clock), and 399-nm (probe) lasers are combined with two dichroic mirrors after transferred by optical fibers. UTC; Coordinated Universal Time, DDS; direct digital synthesizer, SFG; sum-frequency generation, SHG; second harmonic generation, WG-PPLN; waveguided-periodically-poled lithium niobate, AOM; acousto-optic modulator, ECDL; external-cavity diode laser, F-P LD; Fabry- Pérot laser diode, YDFA; ytterbium-doped fiber amplifier, DM; dichroic mirror, PBS; polarizing beam splitter.

The 556-nm light for the green-MOT was obtained by the second harmonic generation (SHG). The output power of 20 mW from an ECDL (Toptica; DL100) at 1112 nm was amplified by a commercial Yb-doped fiber amplifier (YDFA, Keyopsys; KPS-CUS-YFA-1111-SLM-10-PM-CO) up to 200 mW and converted to 556-nm light with an output power of 50 mW by using a ridge-type waveguided periodically-poled lithium niobate (WG-PPLN) crystal. As the natural linewidth of the transition for the green-MOT is $\gamma = 2\pi \times 182$ kHz, the linewidth of the ECDL was narrowed to about 10 kHz by the Pound-Drever-Hall technique [34] with an optical cavity (finesse 10,000). Then, the frequency of the 556-nm laser system was stabilized to the $^1S_0(F = 1/2) - ^3P_1(F = 3/2)$ transition by side-of-fringe locking to a

fluorescence signal from the atomic beam, of which error signal was fed-back to the piezoelectric transducer (PZT) attached to a mirror of the optical cavity. The linewidth of the fluorescence signal was about 6 MHz due to the residual Doppler broadening. However, with the help of the laser power stabilization, the frequency drift was minimized, so that the number and the temperature of ^{171}Yb atoms of the green-MOT could be kept stable for more than one day.

The lattice laser was obtained from a commercial Ti:sapphire laser system (Coherent Inc.; MBR-110) pumped with a single-mode, 532-nm laser (Coherent Inc.; Verdi-V18), producing the output power up to 3 W at 759 nm. Its frequency was stabilized to an internal reference cavity, and was continuously measured using a calibrated commercial wavelength-meter with an accuracy of 10 MHz. After passing through an optical isolator, an AOM for the power stabilization, and a single-mode optical fiber for mode cleaning, a vertical 1-D optical lattice was formed with the laser power up to 0.8 W at 759 nm.

The clock laser at 578 nm was obtained from the sum-frequency generation (SFG) of a 1030-nm fiber laser with 20 kHz linewidth (Koheras; ADJUSTIK) and a 1319-nm Nd:YAG laser with 1 kHz linewidth (Innolight; Mephisto). A WG-PPLN was pumped simultaneously by the co-propagating 1030-nm laser of 10 mW and the 1319-nm laser of 20 mW producing a collimated output beam of 2 mW at 578 nm (Fig. 2). The SFG output was transferred by using polarization-maintaining single-mode optical fibers to three parts; a super-cavity made of ULE glass for linewidth narrowing, an optical lattice setup for clock spectroscopy, and an optical frequency comb for frequency measurement. Frequency noises originated from the fiber transfers to the super-cavity and to the optical lattice setup were actively compensated [35]. The super-cavity had a finesse of 350,000 and was installed horizontally inside a vacuum chamber with the pressure of 10^{-7} Torr and the temperature of the cavity was stabilized at around 30°C within 1 mK. The vacuum chamber was mounted on an active vibration isolation platform and the whole setup was enclosed by an anti-acoustic chamber with a 20-dB isolation. We should note that the cavity was not supported at the vibration-immune points [36] and the stabilized temperature was away from the temperature for the zero thermal-expansion-coefficient of the ULE spacer. Therefore, the linewidth of the clock laser, whose frequency was stabilized to the cavity, was 80 Hz at 100 ms with considerable frequency noises such as mid-term jitters and frequency drifts. In our experiment, the frequency of the clock laser was simultaneously measured by an optical frequency comb during the acquisition time of the clock transition spectrum.

Two ECDLs at 649 nm and 770 nm with the output power of 20 mW were built for the repumping of the populations in the two excited states to the ground state during the interrogation cycle of the clock transition [37]. The frequencies of the 649-nm and the 770-nm ECDLs were stabilized by using the fluorescence signals from Yb atomic beam apparatus corresponding to the transitions of $^3\text{P}_0$ ($F=1/2$) – $^3\text{S}_1$ ($F=1/2$) and $^3\text{P}_2$ ($F=3/2$) – $^3\text{S}_1$ ($F=1/2$), respectively. A third ECDL at 680 nm was used to populate to the $^3\text{P}_0$ and $^3\text{P}_2$ states in the atomic beam via the transition of $^3\text{P}_1$ ($F=3/2$) – $^3\text{S}_1$ ($F=1/2$) with the help of the frequency-stabilized 556-nm laser.

2.2 Experimental overview

The timing sequence for the experiment is shown in Fig. 3. A furnace containing pieces of natural Yb metal (purity 99.9 %) was heated to 450°C and a collimated Yb atomic beam with seven isotopes was produced at a rate of $\sim 10^{10}/\text{s}$. The velocities of ^{171}Yb atoms were slowed in a 30-cm-long Zeeman slower. Slowing laser had a frequency detuning of -500 MHz from the resonant frequency of the $^1\text{S}_0$ ($F = 1/2$) – $^1\text{P}_1$ ($F = 3/2$) transition (natural linewidth; 28 MHz) with an intensity of $30 \text{ mW}/\text{cm}^2$. We estimated the flux of the slowed ^{171}Yb atoms at the MOT region to be $\sim 10^9/\text{s}$.

The same transition was used for the first stage trapping of ^{171}Yb atoms (blue-MOT). The laser for the blue-MOT had a power of 6 mW per axis with a 15-mm beam diameter. The magnetic field gradient by the MOT-coil was 30 G/cm. Trapped atom number in the blue-MOT was saturated roughly at 10^8 , which was measured by a calibrated photo-multiplier tube (PMT). The number of trapped atoms did not increase

further due to the shadow effect of cold atoms, which broke the intensity balance between the incident and the retro-reflected cooling lasers and made the atom cloud unstable. Even though the loading time constant of the blue-MOT was 410 ms, we used 180 ms to reduce the cycle time. It is noted that the blue-MOT stage could be reduced to 80 ms without significantly losing the SNR of the clock signal. Such quick loading time enabled our frequency measurement cycle to be as fast as 5 Hz. It is expected that such a fast interrogation cycle can improve the short-term stability of the optical lattice clock by reducing the Dick effect [38-41].

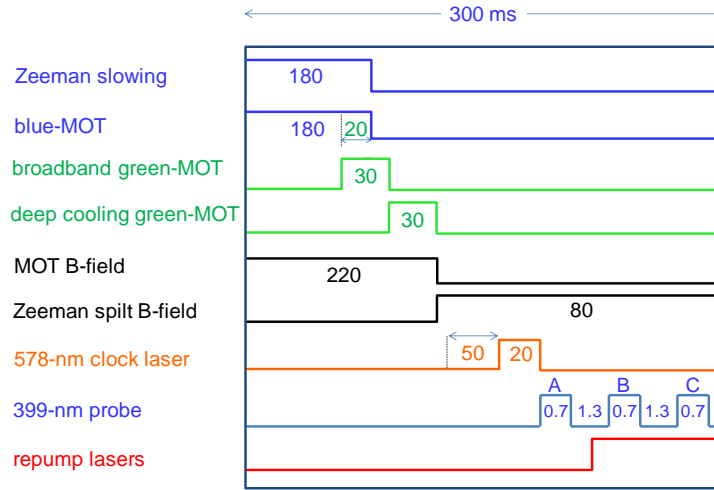


Figure 3. Timing sequence of the experiment for the interrogation of the clock transition of Yb atoms in an optical lattice. (time unit; ms)

The Doppler temperature limit of the blue-MOT is about 0.7 mK, which is much higher than the potential depth of the optical lattice. Therefore, we utilized the second stage trapping (green-MOT) by using the $^1S_0 (F = 1/2) - ^3P_1 (F = 3/2)$ intercombination transition at 556 nm with a narrow linewidth (182 kHz), and the corresponding Doppler temperature limit is 4 μ K. This stage was divided into two steps as shown in Fig. 3. In the first step for 30 ms, a relatively high intensity (3 mW/cm² per axis) of the green-MOT laser, with the frequency detuned (-2 ~ -3 MHz) and modulated (2-MHz depth), was used to increase the atom number transferred from the blue-MOT to the green-MOT. At the end of this step, typically about 70% of the atoms trapped by the blue-MOT were transferred to the green-MOT with temperature of 100 μ K. In the second step for 30 ms, for the purpose of deep cooling, the power of the green-MOT laser was lowered to 0.5 mW per axis, the frequency modulation was turned off, and the center frequency was detuned to about -100 kHz from the resonance frequency. The gradient of the MOT magnetic field was maintained to be 30 G/cm throughout the green-MOT stage.

After the green-MOT stage, atoms were cooled down to about 30 μ K, and the green-MOT laser was turned off using the AOM and a mechanical shutter. A linearly polarized lattice laser at 759 nm was aligned vertically and turned on always during the whole measurement sequences. The laser was focused with an achromatic lens with a focal length of 150 mm and retro-reflected from a concave mirror. It has a dichroic coating for the 759-nm light with a high reflectance and for the 578-nm light with a high transmittance. The beam waist of the focused lattice laser was 25 μ m and the potential depth of the lattice was about 400 E_r , where E_r is the recoil energy of the lattice laser with $E_r/k_B \approx 100$ nK. In this way, roughly 1% of the atoms (10^5) could be transferred to the 1-D lattice from the green-MOT. The corresponding motional sideband frequencies of the longitudinal and the radial motion in the lattice potential were estimated to be 50 kHz and 200 Hz, respectively. The lifetime of trapped atoms in the lattice was measured to be about 400 ms. The shot-to-shot number fluctuation of trapped atoms in the

lattice was typically around 30%.

In the next stage, the clock transition, $^1S_0(F = 1/2) - ^3P_0(F = 1/2)$, was probed. The MOT-field was turned off by a MOSFET switch, and a small bias B-field of 4.3 G was turned on by using a pair of rectangular coil to split the two π -transitions. The spatial inhomogeneity of the B-field was estimated to be less than 1% in the region of the lattice trap and the current fluctuation in the coil was controlled also within 1%. In order to avoid the ringing of the B-field immediately after the MOT-field was turned off, we waited 50 ms before introduction of the clock laser. The direction of the bias B-field and the polarization of the clock laser allow only π -transitions among the Zeeman sub-levels. The clock laser was on for 20 ms with power of 100 nW. Longer interrogation time did not reduce the linewidth of the spectrum due to the broad short-term linewidth (80 Hz) and frequency jitter of the clock laser. Clock laser was co-aligned with the lattice laser within 1-mrad accuracy and the spot size at the interaction region was 90 μm , so that it provided quite a uniform electric field for trapped atoms. The frequency of the clock laser was scanned typically with a 10-Hz step by a direct digital synthesizer (DDS), which drove a double-pass AOM.

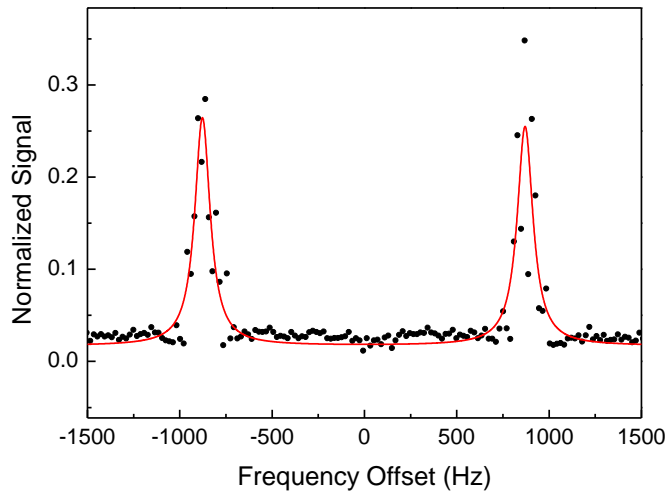


Figure 4. Typical normalized spectrum of the clock transition obtained by single scan of the clock laser. The direction of bias B-field and the polarization of the clock laser allow only π -transitions. Red solid-line is the fit result of the spectrum with a double-peak-Lorentzian function.

The excitation probability of the clock transition was detected by measuring the fluorescence signal from the atoms excited by a 399-nm ECDL resonant to the $^1S_0 - ^1P_1$ transition, known as the electron shelving technique [33]. Since the transition strength is strong enough, all the atoms in the ground state could be swept out within 0.7 ms and the fluorescence signal was detected by a PMT. The fluorescence signal was integrated with a gated integrator for 0.4 ms (signal A). Excited state atoms were transferred to the ground state by using two repumping lasers at 649 nm and 770 nm resonant to the $^3P_0(F=1/2) - ^3S_1(F=1/2)$ and $^3P_2(F=3/2) - ^3S_1(F=1/2)$ transitions, respectively. After the atoms were pumped to the ground state, the fluorescence signal was detected again (signal B). Third integrated signal (signal C) was used to eliminate the background noise. Dominant background noise was due to the scattered photons from the atomic beam. The normalized signal S_N was calculated from the relation $S_N = \frac{b}{a+b}$, where $a = A - C$ and $b = B - C$. Figure 4 shows a typical spectrum of the clock transition obtained by single scan of the clock laser. About 25% of the atoms were excited at resonance, because we did not use the optical pumping between the two Zeeman sub-levels. Center frequencies of two π -transitions were separated by 1.8 kHz due to the applied bias B-field and the typical linewidth of the spectrum of the clock

transition was about 200 Hz dominated by the frequency jitter of the clock laser. To find the clock transition frequency, we fitted the spectrum with a double-peak-Lorentzian function, and obtained the average value of the two frequencies. The clock laser frequency was simultaneously measured by using an optical frequency comb referenced to a H-maser.

3. Evaluation of systematic frequency shifts

To evaluate the light shift due to the lattice laser, we first determined the magic frequency at which the ac Stark shift of the clock transition due to the lattice laser vanishes. As shown in Fig. 5(a), the frequency shift of the clock transition was measured by varying the lattice laser power from 0.3 W to 0.8 W at five different frequencies evenly spaced by 10 GHz around the center frequency of 394 798.33 GHz. Each data point in Fig. 5(a) was obtained from the average value of 40 measurements of the clock transition. Differential shifts for various lattice laser frequencies were obtained (Fig. 5(a)) and fitted to find the magic frequency (Fig. 5(b)) as 394 798.48 (79) GHz, which agrees well with the previous reports [17, 18]. In our absolute frequency measurements, we fixed the lattice laser frequency at 394 798.33 GHz, which was -150 MHz away from the determined magic frequency and the lattice beam power at 680 mW, a frequency shift of 1.3 Hz with an uncertainty of 7.3 Hz was given in the uncertainty budget as shown in Table 1.

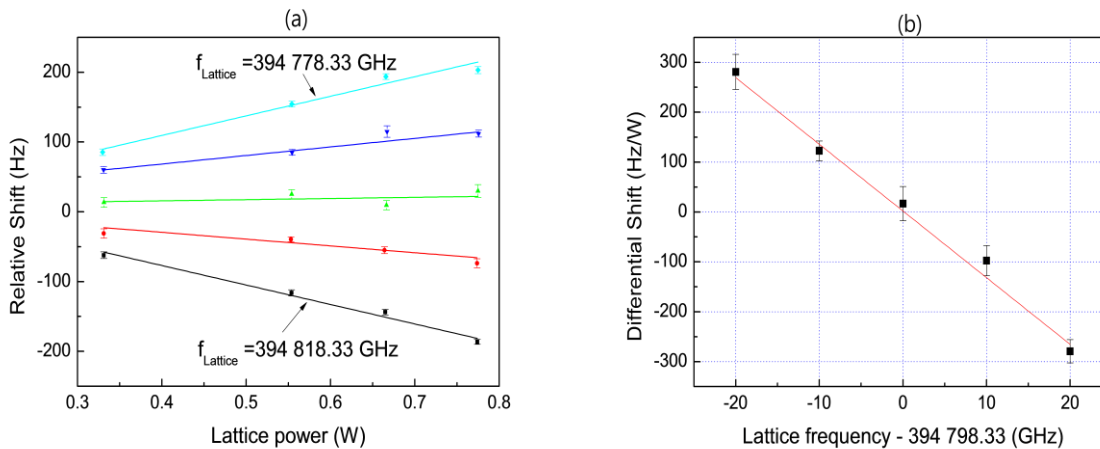


Figure 5. (a) Frequency shift of the clock transition depending on the lattice laser power at five different frequencies of the lattice laser evenly spaced by 10 GHz around the center frequency of 394 798.33 GHz. (b) The differential shift at five frequencies of lattice laser; each point was obtained by the slope from the linear fit at a given frequency of the lattice laser.

Since hyperpolarizability shift could not be measured within our measurement uncertainty, we did not correct this frequency shift. However we estimated the uncertainty from the results obtained by other group with better precision [14, 18], in which the frequency shift was measured to be 0.17(4) Hz at 500 E_r depth. We conservatively estimated the associated uncertainty to be 0.2 Hz without correcting the shift, considering the reported shift and the shallower lattice potential depth of 400 E_r used in our experiments.

The vector-polarizability-induced shift disappears with linearly polarized light [16]. Although small amount of the polarization ellipticity can take place due to the birefringence of mirrors and vacuum windows, vector shift can be suppressed to less than 10^{-18} by the use of linear polarization, cancellation due to the averaging process of two π -transitions, and experimental geometry [18]. Therefore, we did not correct the vector shift in Table 1.

The first-order Zeeman shift was also cancelled by taking the average frequency of the two π -transitions in Fig. 4. However, the second-order Zeeman shift depends on the square of the magnetic field intensity, and it cannot be cancelled in this way. Using the value of the bias B-field of 4.3 G measured

from the Zeeman splitting and the second-order Zeeman coefficient of $-0.07(1) \text{ Hz/G}^2$ [18], the frequency shift due to the second-order Zeeman effect was estimated to be $-1.3(2) \text{ Hz}$.

The blackbody radiation shift was evaluated by measuring the temperature and the fractional solid angles (FSA) of the components surrounding the atoms in the lattice trap as discussed in Ref. [42]. Considering the stainless steel vacuum chamber ($36\sim 43^\circ\text{C}$, $\text{FSA}=0.9$), the view-port windows ($26\sim 29^\circ\text{C}$, $\text{FSA}=0.1$), and the furnace for the atomic beam ($452(5)^\circ\text{C}$, $\text{FSA}=0.01$), the frequency shift due to the blackbody radiation was estimated to be $-1.6(3) \text{ Hz}$.

The gravitational shift was evaluated using the height of the lattice trap (92.0 m) from the geoid, which was measured by a GPS antenna. The frequency shift to the gravity was estimated to be $5.2(1) \text{ Hz}$.

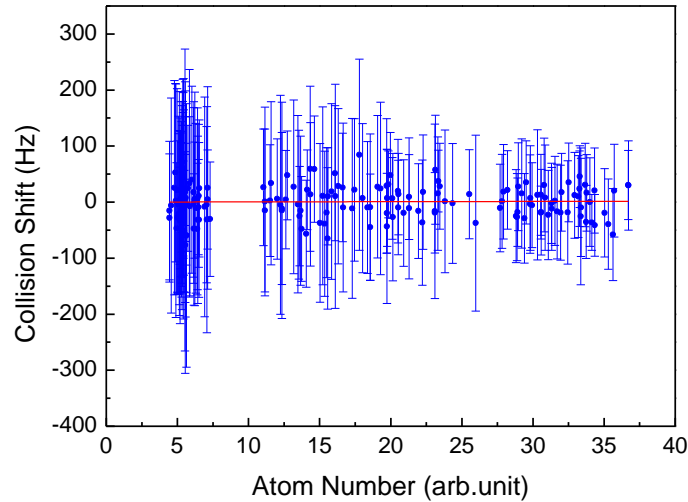


Figure 6. Measurement of collision shift of the clock transition. Red solid line is a linear fit to the data points.

The collision shift should be included in the uncertainty budget, because approximately 10^5 atoms were captured in several hundred lattice sites and the estimated density was higher than $10^{11}/\text{cm}^3$. Since the atoms in a lattice were not spin-polarized in our measurements, s-wave collision between the ground state atoms was not forbidden. Recent result [19] has shown that the collision shift of the un-polarized atoms is smaller than that of the spin-polarized ones, implying that competing interactions have the opposite sign as those in the polarized case. However, the excitation fraction was not fixed in our experiment, since the clock laser frequency was not locked at a specified excitation fraction but was scanned across the resonance peak to get the clock transition spectrum. Therefore, only the averaged shift for different excitation fractions could be measured. To experimentally determine the collision shift, we varied atom numbers by interleaving the loading time of the blue-MOT from 80 to 680 ms. The atom number (with an arbitrary unit) was measured by using the integrated fluorescence signals (A , B in Fig. 3) of the 399-nm probe light, which were described in section 2.2. As shown in Fig. 6, the linear least-square-fit result gives the slope of 0.04 with the uncertainty of 0.20, which means that the density shift could not be clearly observed within our frequency measurement uncertainty. Under the typical experimental condition of our frequency measurement at an atom number of $14(3)$ in this arbitrary unit, the collision shift was estimated to be 0.6 Hz with the uncertainty of 2.7 Hz .

The light shift due to the clock laser can be estimated from the previous results [15]. If we adopt the reported measured coefficient and the clock laser power of $1.6 \text{ mW}/\text{cm}^2$ used in this work, the shift is negligible (less than 30 mHz). The other systematic effects, such as the residual Doppler shift and the AOM phase chirp, are estimated to be negligibly small within our frequency measurement uncertainty.

Table 1. Uncertainty budget for the absolute frequency measurement of the ^{171}Yb optical lattice clock.

Effect	Shift(Hz)	Uncertainty(Hz)	Relative Uncertainty($\times 10^{-15}$)
Linear lattice ac Stark shift	1.3	7.3	14
Hyperpolarizability	0	0.2	0.4
Second order Zeeman	-1.3	0.2	0.4
Gravitational shift	5.2	0.1	0.2
Blackbody radiation shift	-1.6	0.3	0.6
Collisional shift	0.6	2.7	5.2
Total Yb	4.2	7.8	15
Statistical	-	1.0	1.9
H-maser link to UTC	-	4.7	9.1
Total	4.2	9.2	18

4. Absolute frequency determination

To measure the absolute frequency of the clock transition, we measured the frequency of the clock laser by using an optical frequency comb referenced to a H-maser. The frequency offset of the H-maser from the UTC and the frequency shifts due to the systematic effects, which were discussed in section 3, were compensated.

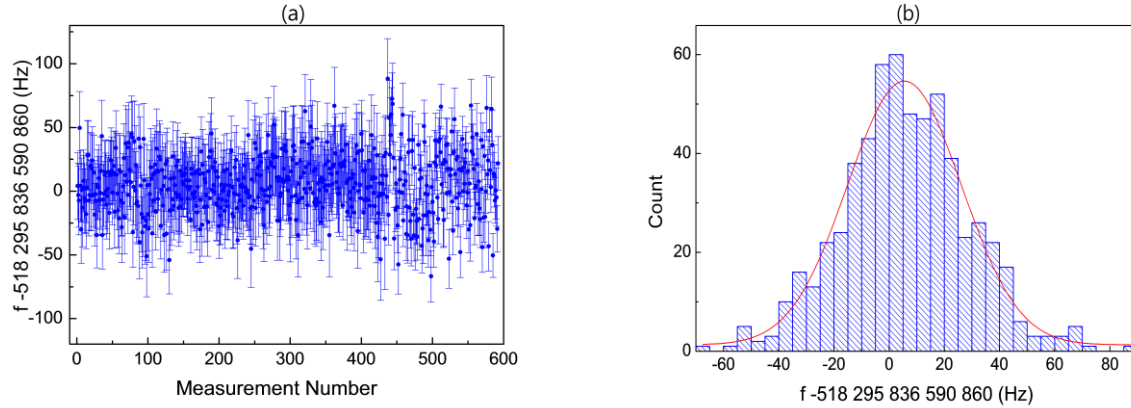


Figure 7. (a) 592 measurement results of the absolute frequency of the clock transition after correcting the frequency shift by the systematic effects and the H-maser offset from the UTC. (b) Histogram of the frequency measurements in (a) and its Gaussian fit.

592 measurement results in total were used for absolute frequency measurement, and the result is shown in Fig. 7(a) after the correction of the systematic shifts and the H-maser offset from the UTC. The resulting statistical uncertainty associated with the measurement of the clock transition was 1.0 Hz. The histogram of the frequency measurements is well fitted by a Gaussian distribution as in Fig. 7(b). The frequency-transfer uncertainty in the correction of the H-maser frequency offset from the UTC was estimated to be 4.7 Hz following the process in Ref. [43]. The systematic shifts and associated uncertainties are summarized in Table 1. The total systematic uncertainty was 7.8 Hz (1.5×10^{-14}). Lattice-induced ac-Stark shift and collision shift uncertainties were major contributions to the total systematic uncertainty. Including the uncertainty related to the H-maser offset from the UTC, the absolute frequency of the clock transition was determined to be 518 295 836 590 865.7 Hz with an uncertainty of 9.2 Hz

(1.8×10^{-14}). This result is compared with the two previous measurements by other group in Fig. 8, which shows good agreement within the uncertainty of this work.

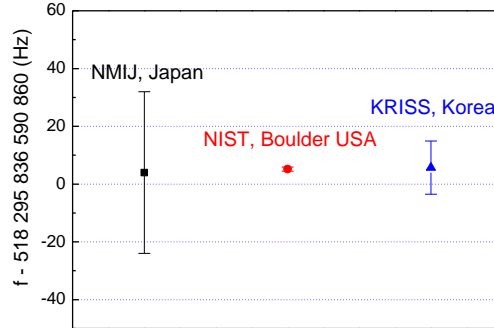


Figure 8. Measurement results of the absolute frequency of the ^{171}Yb lattice clock transition by different institutes: NMIJ [17], NIST [18], and KRISS (this work).

5. Conclusion

We measured the absolute frequency of the $^1S_0(F = 1/2) - ^3P_0(F = 1/2)$ transition of ^{171}Yb atoms confined in a 1-D optical lattice. The determined frequency was 518 295 836 590 865.7 Hz with an uncertainty of 9.2 Hz (1.8×10^{-14}). The frequency is in good agreement with the results of previous measurements of other laboratories within the uncertainty of this work. As a third independent measurement, our measurement result would contribute to reduce the recommended frequency uncertainty of this clock transition as a secondary representation of the second.

To reduce the current frequency measurement uncertainty, which is limited mainly by the clock laser instability, an improved clock laser system with better stability will be employed in the near future. Also, a Cs fountain clock is under development at KRISS, with which the uncertainty due to the frequency transfer from the UTC can be eliminated. We expect that a more precise frequency measurement is within our reach after these improvements and direct comparison of optical lattice clocks with other laboratories become possible.

Acknowledgements

We gratefully acknowledge the experimental assistance from Masami Yasuda during his stay at KRISS and helpful discussions with Feng Lei Hong from NMIJ.

Reference

- [1] Takamoto M, Hong F-L, Higashi R and Katori H 2005 *Nature* **435** 321-4
- [2] Ludlow A D, Boyd M M, Zelevinsky T, Foreman S M, Blatt S, Notcutt M, Ido T and Ye J 2006 *Phys. Rev. Lett.* **96** 033003
- [3] Targat R L, Baillard X, Fouché M, Bruschi A, Tcherbakoff O, Rovera G D and Lemonde P 2006 *Phys. Rev. Lett.* **97** 130801
- [4] Takamoto M, Hong F, Higashi R, Fujii Y, Imae M and Katori H 2006 *J. Phys. Soc. Japan* **75** 104302

- [5] Boyd M M, Ludlow A D, Blatt S, Foreman S M, Ido T, Zelevinsky T and Ye J 2007 *Phys. Rev. Lett.* **98** 083002
- [6] Ludlow A D, Zelevinsky T, Campbell G K, Blatt S, Boyd M M, de Miranda M H G, Martin M J, Thomsen J W, Foreman S M, Ye J, Fortier T M, Stalnaker J E, Diddams S A, Le Coq Y, Barber Z W, Poli N, Lemke N D, Beck K M and Oates C W 2008 *Science* **319** 1805-8
- [7] Baillard X, Fouché M, Le Targat R, Westergaard P G, Lecallier A, Chapelet F, Abgrall M, Rovera G D, Laurent P, Rosenbusch P, Bize S, Santarelli G, Clairon A, Lemonde P, Grosche G, Lipphardt B and Schnatz H 2008 *Eur. Phys. J. D* **48** 11-7
- [8] Campbell G K, Ludlow A D, Blatt S, Thomsen J W, Martin M J, de Miranda M H G, Zelevinsky T, Boyd M M, Ye J, Diddams S A, Heavner T P, Parker T E and Jefferts S R 2008 *Metrologia* **45** 539-48
- [9] Westergaard P G, Lodewyck J, Lorini L, Lecallier A, Burt E A, Zawada M, Millo J and Lemond P 2011 *Phys. Rev. Lett.* **106** 210801
- [10] Swallows M D, Bishof M, Lin Y, Blatt S, Martin M J, Rey A M and Ye J 2011 *Science* **331**, 1043-6
- [11] Falke St, Schnatz H, Winfred J S R V, Middelman Th, Vogt St, Weyers S, Lipphardt B, Grosche G, Riehle F, Sterr U and Lisdat Ch 2011 *Metrologia* **48** 399-407
- [12] Hoyt C W, Barber Z W, Oates C W, Fortier T M, Diddams S A and Hollberg L 2005 *Phys. Rev. Lett.* **95** 083003
- [13] Barber Z W, Hoyt C W, Oates C W, Hollberg L, Taichenachev A V and Yudin V I 2006 *Phys. Rev. Lett.* **96** 083002
- [14] Barber Z W, Stalnaker J E, Lemke N D, Poli N, Oates C W, Fortier T M, Diddams S A, Hollberg L and Hoyt C W 2008 *Phys. Rev. Lett.* **100** 103002
- [15] Poli N, Barber Z W, Lemke N D, Oates C W, Ma L-S, Stalnaker J E, Fortier T M, Diddams S A, Hollberg L, Bergquist J, Bruschi A, Jefferts S, Heavner T and Parker T 2008 *Phys. Rev. A* **77** 050501(R)
- [16] Porsev S G, Derevianko A and Fortson E N 2004 *Phys. Rev. A* **69** 021403(R)
- [17] Kohno T, Yasuda M, Hosaka K, Inaba H, Nakajima Y and Hong F-L 2009 *Appl. Phys. Express* **2** 072501
- [18] Lemke N D, Ludlow A D, Barber Z W, Fortier T M, Diddams S A, Jiang Y, Jefferts S R, Heavner T P, Parker T E and Oates C W 2009 *Phys. Rev. Lett.* **103** 063001
- [19] Ludlow A D, Lemke N D, Sherman J A, Oates C W, Quéméner G, von Stecher J and Rey A M 2011, *Phys. Rev. A* **84** 052724
- [20] Petersen M, Chicireanu R, Dawkins S T, Magalhães D V, Mandache C, Le Coq Y, Clairon A and Bize S 2008 *Phys. Rev. Lett.* **101**, 183004
- [21] Mejri S, McFerran J J, Yi L, Le Coq Y and Bize S 2011 *Phys. Rev. A* **84** 032507
- [22] Yi L, Mejri S, McFerran J J, Le Coq Y and Bize S 2011 *Phys. Rev. Lett.* **106** 073005
- [23] Friebe J, Riedmann M, Wübbena T, Pape A, Kelkar H, Ertmer W, Terra O, Sterr U, Weyers S, Grosche G, Schnatz H and Rasel E M 2011 *New J. Phys.* **13** 125010
- [24] Leibfried D, Blatt R, Monroe C and Wineland D 2003 *Rev. Mod. Phys.* **75** 281-324
- [25] Oskay W H, Diddams S A, Donley E A, Fortier T M, Heavner T P, Hollberg L, Itano W M, Jefferts S R, Delaney M J, Kim K, Levi F, Parker T E and Bergquist J C 2006 *Phys. Rev. Lett.* **97** 020801
- [26] Chou C W, Hume D B, Koelemeij J C J, Wineland D J and Rosenband T 2010 *Phys. Rev. Lett.* **104** 070802
- [27] Szymaniec K, Park S E, Marra G and Chalupczak W 2010 *Metrologia* **47** 363-76
- [28] Li R, Gibble K and Szymaniec K 2011 *Metrologia* **48** 283-9
- [29] Wynands R and Weyers S 2005 *Metrologia* **42** S64-79
- [30] Hong F-L, Inaba H, Hosaka K, Yasuda M and Onae A 2009 *Opt. Express* **17** 1652-9
- [31] Nevsky A U, Bressel U, Ernsting I, Eisele Ch, Okhapkin M, Schiller S, Gubenko A, Livshits D, Mikhrin S, Krestnikov I and Kovsh A 2008 *Appl. Phys. B* **92** 501-7
- [32] Lee W-K, Park C Y, Yu D-H, Park S E, Lee S-B and Kwon T Y 2011 *Opt. Express* **19** 17453-61

- [33] Dehmelt H 1975 *Bull. Am. Phys. Soc.* **20**, 60
- [34] Drever R W P, Hall J L, Kowalski F V, Hough J, Ford G M, Munley A J, and Ward H 1983 *Appl. Phys. B* **31** 97-105
- [35] Ma L-S, Jungner P, Ye J and Hall J L 1994 *Opt. Lett.* **19** 1777-9
- [36] Webster S A, Oxborrow M and Gill P 2007 *Phys. Rev. A* **75** 011801(R)
- [37] Cho J W, Lee H-G, Lee S, Ahn J, Lee W-K, Yu D-H, Lee S K and Park C Y 2011 <http://arxiv.org/abs/1111.6225>
- [38] Dick G 1987, "Local oscillator induced instabilities in trapped ion frequency standards," in Proc. of Precise Time and Time Interval, Redondo Beach, pp. 133–147
- [39] Santarelli G, Audoin C, Makdissi A, Laurent P, Dick G J and Clairon A 1998 *IEEE Trans. Ultrason. Ferroelect. Freq. Contr.* **45** 887–94
- [40] Quessada A, Kovacich R P, Courtillot I, Clairon A, Santarelli G and Lemonde P 2003 *J. Opt. B* **5** S150-4
- [41] Westergaard P G, Lodewyck J and Lemonde P 2010 *IEEE Trans. Ultrason. Ferroelect. Freq. Contr.* **57** 623–8
- [42] Porsev S G and Derevianko A 2005 *Phys. Rev. A* **74** 020502(R)
- [43] Panfilo G and Parker T E 2010 *Metrologia* **47** 552-60